


Article

Bio-Polyamide 11 Hybrid Composites Reinforced with Basalt/Flax Interwoven Fibers: A Tough Green Composite for Semi-Structural Applications

Pietro Russo ^{1,*} , Giorgio Simeoli ¹, Libera Vitiello ² and Giovanni Filippone ^{2,*} 

¹ Institute for Polymers, Composites and Biomaterials—National Council of Research, 80078 Pozzuoli, Naples, Italy; giorgio.simeoli@unina.it

² Department of Chemical, Materials and Production Engineering, University of Naples Federico II, 80125 Naples, Italy; liberavitiello29@gmail.com

* Correspondence: pietro.russo@unina.it (P.R.); gfilippo@unina.it (G.F.)

Received: 11 March 2019; Accepted: 29 April 2019; Published: 6 May 2019



Abstract: Intraply hybrid green composites were prepared by film stacking and hot-pressing of bio-based polyamide 11 (PA11) sheets and commercial hybrid fabrics made by interweaving flax and basalt fibers (2/2 twill structure). Two matrices were considered, one of them containing a plasticizing agent. After preliminary thermal and rheological characterizations of the neat matrices, the laminates were studied in terms of flexural properties at low and high deformation rates, and the results were interpreted in the light of morphological analyses (scanning electron and optical microscopy). Despite the poor interfacial adhesion detected for all investigated composite samples, the latter exhibited a good combination of flexural strength, modulus, and impact resistance. Such well-balanced mechanical properties make the studied samples potential candidates for semi-structural applications, e.g., in the transportation sector.

Keywords: polyamide 11; interweaving flax-basalt fibers; hybrid composites; flexural properties

1. Introduction

In the last decades, a steady increase of interest has been devoted toward the design and development of hybrid composite systems given their outstanding perspectives of applications, even for advanced uses, deriving from the ability to combine advantages of the individual constituents, for example, stiffness and toughness, and the occurrence of synergisms, not yet well understood [1–4].

In line with the general trend to use reinforced plastics for both functional and structural applications, the hybridization approach, mainly obtained by embedding two or more different fibers within a polymer matrix, allows to tailor the properties of products to suit ever more specific requirements. In this regard, common configurations consist of different kinds of fibers distributed in different laminas or in the same one to form interply or intraply hybrids, respectively [5,6].

Gonzales et al. [7] focused on the low-velocity impact behavior of polymer-based interply hybrid laminates including woven carbon fabric, woven glass fabric, and unidirectional carbon tapes. Authors demonstrated that the stacking sequence of constituting layers can significantly affect results and failure mechanisms. In particular, the dissipation of impact energy is reduced when the woven fabrics are placed in the mid-plane of the studied composite structure, with a simultaneous increase of the residual properties. Ying et al. [8] studied the influence of hybridization on the impact properties of carbon-aramid/epoxy systems. Experimental tests highlighted that placing a high stiffness carbon fabric in correspondence of highly resistant regions permits to achieve enhanced properties of the reinforcement. Ferrante et al. [9] considered the effect of basalt fibers hybridization on the damage

tolerance of carbon/epoxy laminates subjected to laser shock wave tests. The research indicated an optimal behavior for sandwich-like configurations, especially in the case of structures with basalt skins. Nisini et al. [10] analyzed ternary systems including carbon, basalt and flax fibers in an epoxy matrix obtained according to two different configurations. Samples were subjected to tensile, flexural, interlaminar shear strength and low-velocity impact tests. The inclusion of flax fibers showed a significant effect especially with regard to impact response of investigated materials.

Nowadays, the growing sensitivity towards environmental issues has increasingly moved the attention of researchers and industrials towards inherently recyclable materials and/or based on constituents coming from renewable sources. According to this consideration, the use of eco-sustainable thermoplastic resins and natural reinforcements is rapidly gaining a significant role even in industrial fields where the use of traditional carbon fiber- and glass fiber-reinforced thermosetting materials is widely established (aeronautics, naval, construction). Unfortunately, both natural fibers and low environmental impact plastics often suffer from poor performance, and their combination consequently results in “green composites” that do not meet the necessary requirements for many technologically relevant applications. The challenge is identifying new combinations of raw materials for the production of green composites whose performance is good enough to propose their use in suited applications. Among the various bio-based thermoplastic resins here we focus our attention on polyamide 11 (PA11), which is a semi-crystalline bio-polyamide produced using 11-aminoundecanoic acid derived from castor oil. Despite its relatively high costs, in the last decade, PA11 has gained a special industrial interest due to a good combination of mechanical properties and chemical resistance. In particular, PA11 exhibits good toughness compared to other bio-based thermoplastic resins, e.g., poly(lactic acid), which is often proposed as a matrix for bio-composites [11–15]. As far as the fibers are concerned, here we deal with a hybrid fabric made of basalt and flax interwoven fibers in 2/2 twill structure. This class of reinforcements has gained over time an extraordinary interest in research, as their use in polymeric matrices can offer different possibilities from the triggering of synergisms to mechanical properties not exhibited by composite materials similar but reinforced with each of the two combined fibers, separately [16–18]. The mechanical performance of composite laminates obtained by film stacking is investigated in both static and dynamic conditions. The results, appropriately supported by a morphological investigation of the induced damage, reveal a good combination of flexural properties and toughness, which suggest possible use in semi-structural applications, such as panels for the transportation field.

2. Materials and Methods

2.1. Materials

Two extrusion grade polyamide 11 (PA11) Besno Rilsan[®] from Arkema S.A. (Puteaux, France): a non-plasticised TL (density: 1.03 g/cm³, MFI@235 °C/2.16 kg = 4.38 ± 1.25 g/10 min) and a plasticized P40 TL (density: 1.04 g/cm³, MFI@235 °C/2.16 kg = 4.06 ± 0.61 g/10 min), were considered as matrices.

A hybrid fabric constituted by the interweaving of flax and basalt fibers in equal proportion and purchased at Lincore[®] (Bourguebus, France) with nominal areal weight 360 g/m² and an architecture twill 2/2 type was used as the reinforcement.

2.2. Laminates Preparation

Films with a thickness approximately equal to 80 µm were prepared using a Collin flat die extruder Teach-Line E20T equipped with a calender CR72T (Collin GmbH, Ebersberg, Germany). In detail, filming was conducted at a screw speed of 60 rpm, setting the temperature profile along the screw at 170–210–220–220–200 °C.

Composite laminates were obtained by the film stacking technique according to which PA11 films and hybrid fiber fabrics were alternately stacked and hot-pressed with a lab press Mod. P400E (Collin

GmbH, Ebersberg, Germany) under pre-optimized conditions with a maximum temperature of 225 °C. The molding cycle is shown in Figure 1.

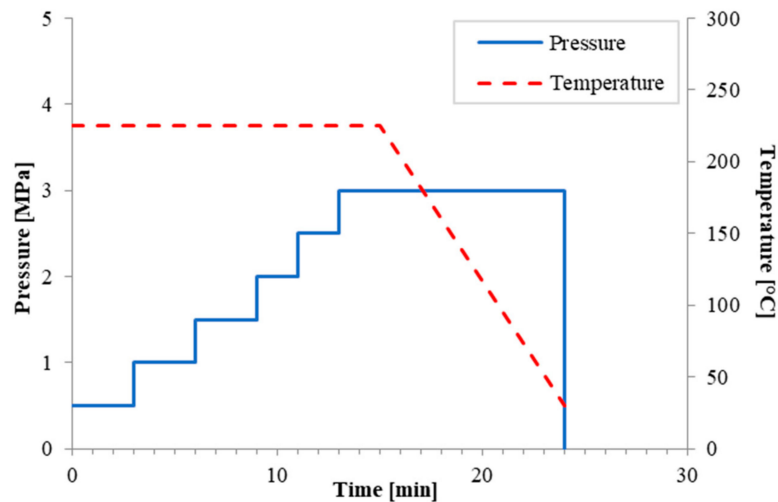


Figure 1. Processing conditions to prepare all PA11 based laminates.

Operating in this way, laminated samples were prepared by stacking four plies with plastic films. The final samples had a thickness approximately equal to 1.95 mm and volume fiber content of about 34%.

2.3. Calorimetric Tests

Differential scanning calorimetry (DSC) tests have been performed using a Q20 (TA Instruments, Milan, Italy) set-up on films of investigated matrices, at a rate of 10 °C/min and on the temperature range from 0 °C to 250 °C. The collected data permitted to assess the glass transition temperature of matrices and their degree of crystallinity according to the following Equation (1):

$$X_c = \frac{\Delta H_m}{\Delta H_{m0}} \quad (1)$$

where ΔH_m is the measured melting enthalpy while ΔH_{m0} is the melting enthalpy of the PA11 fully crystallized (189 J/g) [19].

2.4. Rheological Analysis

The flow behavior of the polymer matrices was investigated through rotational rheometry using a stress-controlled rotational rheometer (AR-G2 by TA Instruments) (Milan, Italy). Oscillatory shear experiments (frequency scans) were carried out to get the elastic (G') and viscous (G'') moduli in the linear viscoelastic regime, whose limits were assessed through preliminary strain amplitude shear tests. The frequency scans were performed in air atmosphere from frequency $\omega = 10^2$ rad/s down to $\omega = 10^{-1}$ rad/s. The strain amplitude was $\gamma = 5\%$ for both PA11 TL and PA11 P40 TL resins. The testing temperatures were $T = 220$ °C for the PA11 TL and $T = 205$ °C for the PA11 P40 TL. This enabled to compare the rheological behavior of the two matrices at the same reduced temperature $\theta = T_{\text{test}} - T_{m-c} \approx 10$ °C (T_{m-c} being the temperature of melting peak closing). Note that lower temperatures were not explored because of the excessive viscosity of the selected matrices.

2.5. Morphological Observations

Morphological analysis was conducted on cryo-fractured surfaces of composite samples to highlight any interfacial feature useful to support mechanical results. In this regard, observations

were captured with a field emission scanning electron microscope (mod. FEI QUANTA 200 F) (Zurich, Switzerland) operating in high vacuum conditions at the voltage of 20 kV. Analyzed surfaces were previously coated with a thin layer of a gold-palladium alloy.

2.6. Static-Mechanical Tests

Tensile and flexural tests were conducted with a Tensometer 2020 (Alpha Technologies, Cinisello Balsamo, Milan, Italy).

In particular, tensile measurements on the neat polymer matrices were performed on dog-bone shaped specimens, obtained by compression molding, according to the ASTM D638-14. Five specimens were tested at room temperature, with a displacement rate of 5 mm/min and using a load cell of 10 kN.

Flexural tests were carried out on both neat matrices and laminates. The measurements were performed loading each specimen up to 5% of strain, according to the ASTM D790-03, by using a load-cell of 500 N. The reported results represent average values computed from five independent measurements per each sample.

2.7. Charpy-Like Tests

High-velocity flexural properties of the laminates were estimated by means of an instrumented Charpy impact testing machine CEAST 9500 (ITW Test and Measurements, Pianezza, Turin, Italy). Three-point bending tests were performed on five specimens with a length approximately equal to 100 mm and using a span width of 62 mm, at a load application speed of 3.8 m/s. Results are reported in terms of stress-deformation curves.

3. Results

The main calorimetric properties collected through DSC analysis are summarized in Table 1. The plasticizing agent present in the sample PA11 P40 TL causes the reduction of the glass transition temperature, which passes from $T_g = 50.5$ °C to $T_g = 37.7$ °C. Besides this expected reduction of T_g , the plasticizer also affects the melting peak, which results narrowed and shifted to lower temperatures, with obvious advantages in terms of processability. Furthermore, it is interesting to notice that the melting enthalpy of the two samples is essentially the same and, according to the Equation (1), it corresponds to a degree of crystallinity approximately equal to $\chi \approx 27\%$.

Table 1. Main calorimetric properties of the polymer matrices.

Parameter	PA11 TL	PA11 P40 TL
Glass transition temperature, T_g in °C	50.5	37.7
Melting temperature, T_m (onset/peak/peak closing) in °C	182.6/193.8/210.2	164.7/182.5/195.5
Melting enthalpy, ΔH_m in J/g	50.6	51.3
Degree of crystallinity, χ in %	26.7	27.1

The results of rheological analyses are shown in Figure 2a,b, where G' and G'' are shown as a function of frequency together with the complex viscosity, $\eta^* = \sqrt{G'^2 + G''^2}/\omega$. When compared at the same reduced temperature θ , the samples are almost indistinguishable and share the same phenomenological behavior, characterized by moduli comparable between them in the whole range of investigated frequency. G'' is slightly higher than G' at low frequency, while the moduli cross each other at $\omega \approx 10$ rad/s and G' exceeds G'' for higher frequency. Both moduli apparently approach a plateau value at low frequency. Actually, such behavior is a consequence of polymer degradation during time, which causes a growth of the viscoelastic quantities while testing from high to low frequencies. This can be seen in the insets of Figure 2a,b, where the complex viscosity at $\omega \approx 10$ rad/s is reported as a function of time. In this regard, two aspects can be highlighted: (i) the viscosity of the selected polymers, which can be assumed equivalent to η^* according to the Cox–Merz rule,

is very high, being of order of $\sim 10^4$ Pa s in the range of shear rate typically experienced during the film stacking step for the preparation of the laminates (i.e., $\dot{\gamma} \sim 5$ 1/s, see [20]), (ii) the viscosity grows quite rapidly over time. This rheological information is precious when considering the efficacy of the film stacking step and the mechanical performance of the laminates. First of all, the film stacking process was carried out at $T = 190$ °C, which is a lower temperature than that of rheological tests. It is hence reasonable to expect that the viscosity of both matrices during laminate preparation was even higher than that measured via rheological tests. The effect of such a high viscosity of the matrices is a delay in the permeation times of the polymer in the fabric, which inversely depends on the viscosity as predicted by the Darcy’s law for the flow in porous mediums. Slow permeation times can have detrimental effects on the level of compaction of the laminates. On the other hand, the solution of prolonging the duration of the hot pressing process is not feasible in this case because of the growth of the viscosity over time (see insets of Figure 2a,b).

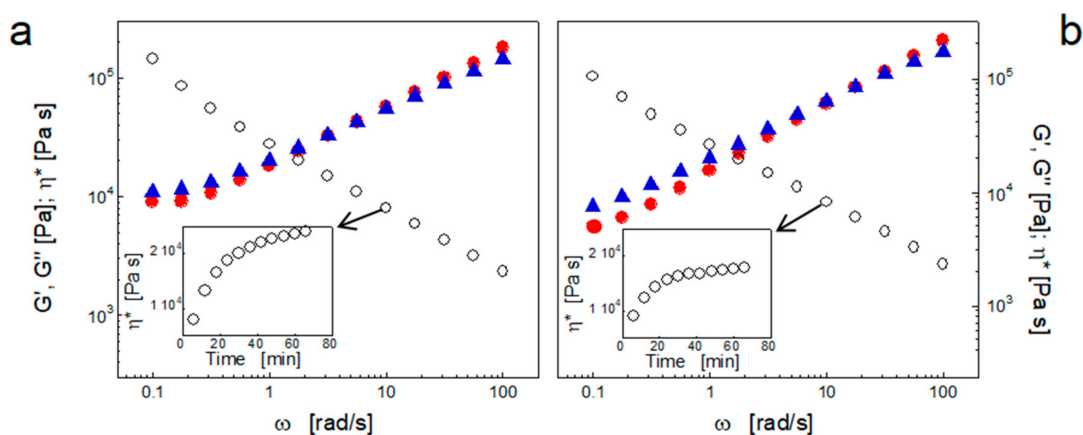


Figure 2. Frequency dependence of G' (red circles), G'' (blue triangles), and η^* (empty circles) for PA11 TL (a) and PA11 P40 TL (b) at $\theta \approx 10$ °C. The time evolution of G' (red circles) and G'' (blue triangles) at $\omega = 10$ rad/s is shown in the insets.

Figure 3 shows the tensile stress-strain curves of considered polyamides. Clearly, both matrices exhibit a ductile behavior with the non-plasticized polymer showing, as expected, higher tensile modulus and strength, as well as lower deformation at break than the plasticized one.

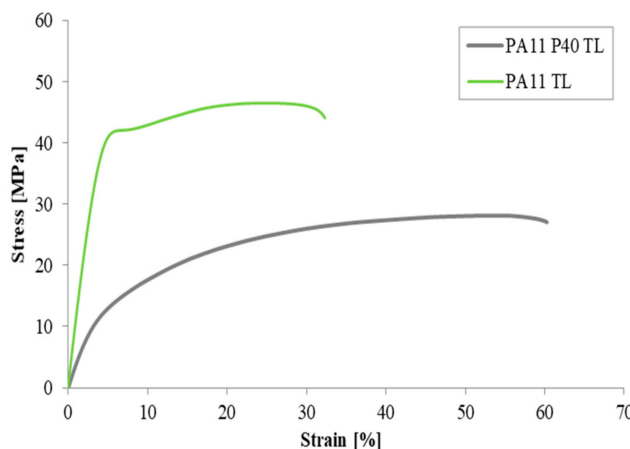


Figure 3. Representative tensile stress-strain curves of PA11 matrices.

The tensile parameters obtained by processing these curves and summarized in Table 2 are in line with data already available in the literature [21].

Table 2. Tensile parameters.

Parameter	PA11 TL	PA11 P40 TL
Young modulus, in GPa	1.01 ± 0.02	0.39 ± 0.02
Yield stress (0.2% offset), in MPa	38.8 ± 3.6	15.5 ± 0.4
Yield strain (0.2% offset), in %	4.9 ± 0.5	7.5 ± 0.5
Tensile strength, in MPa	44.9 ± 0.5	29.4 ± 1.1
Stress at break, in MPa	43.3 ± 2.4	28.8 ± 1.5
Strain at break, in %	26.9 ± 6.6	66.0 ± 5.8
Toughness, in MPa	10.7 ± 3.4	15.9 ± 1.6
Resilience, in MPa	1.56 ± 0.01	0.74 ± 0.08

Similarly, Figure 4 refers to the flexural response of PA11 TL and PA11 P40 TL. In this case, both resins show that the stress, at least on the deformation range foreseen by the reference standard (up to 5%), is continuously increasing. This behavior can be explained on the basis of the ductility of the studied materials and, therefore, of their ability to support the load without yielding until 5% of deformation is reached.

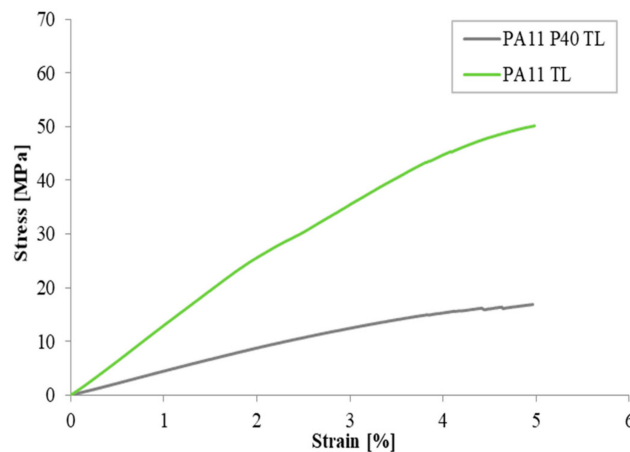
**Figure 4.** Representative flexural stress-strain curves of PA11 matrices.

Table 3, showing the average values and standard deviations of both the elastic modulus and the flexural strength for the two polyamide matrices, confirms that the presence of plasticizers implies, even in the case of flexural loads, a significant reduction in performance. In particular, the flexural stiffness and strength of the plasticized sample are about three times lower respect to the not plasticized one.

Table 3. Flexural parameters of PA11 matrices.

Parameter	PA11 TL	PA11 P40 TL
Flexural modulus, in GPa	1.31 ± 0.11	0.45 ± 0.06
Flexural offset yield strength (0.2% offset), in MPa	30.2 ± 2.4	11.8 ± 1.5
Yield strain (0.2% offset), in %	2.55 ± 0.13	2.72 ± 0.11
Flexural strength, in MPa	>50.3	>17.3

Once the polymer matrices have been characterized, the attention was moved on the laminates. First of all, SEM analyses were performed to investigate the interactions between the fibers and the matrices. The micrographs of the cryo-fractured surfaces of the composite systems are shown in Figure 5. The pictures clearly highlight a poor interfacial adhesion, which suggests the propensity of both the investigated composite systems to undergo dissipative phenomena, such as delamination, when subjected to external loads.

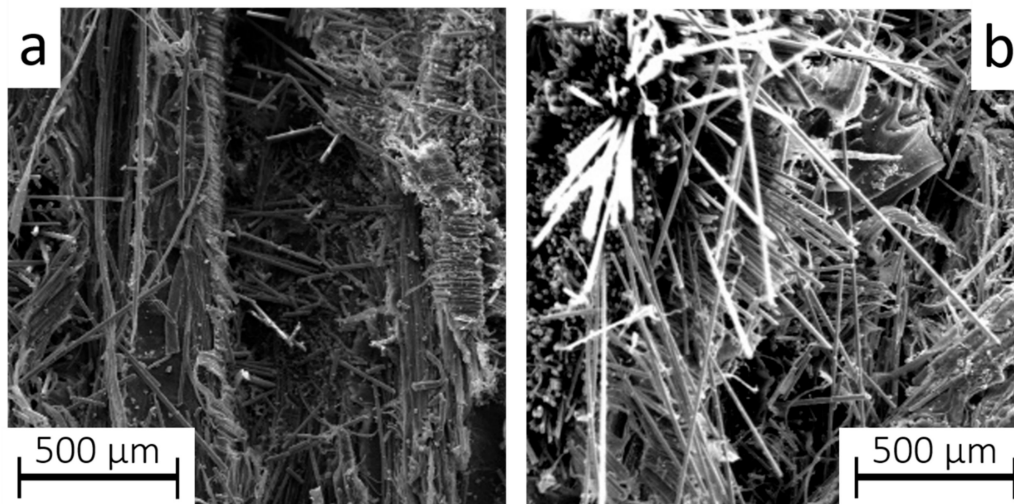


Figure 5. SEM micrographs of (a) PA11 TL and (b) PA11 P40 TL based composites.

The composites were subjected to flexural tests, and the results are shown in Figure 6 in terms of representative stress-strain curves. The numerical results are resumed in the Table 4.

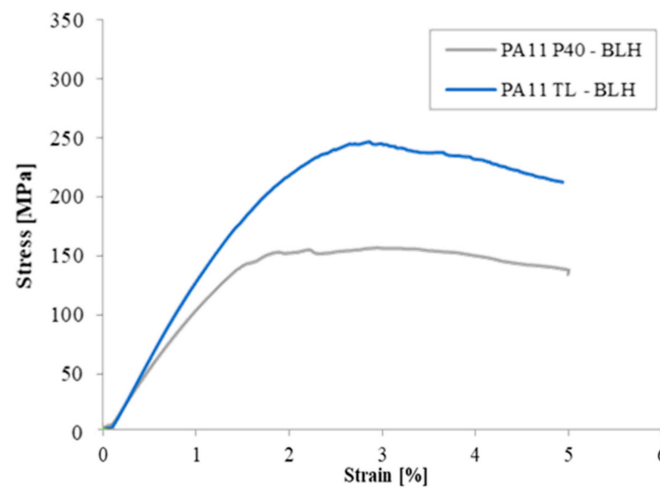


Figure 6. Representative flexural stress-strain curves of PA11 hybrid composites.

Table 4. Flexural parameters of PA11 based composites.

	PA11 TL-BLH	PA11 P40 TL-BLH
Flexural modulus, in GPa	9.1 ± 0.4	7.5 ± 0.2
Flexural offset yield strength (0.2% offset), in MPa	173 ± 8.2	90 ± 7.4
Yield strain (0.2% offset), in %	1.46 ± 0.24	0.82 ± 0.16
Flexural strength, in MPa	250.1 ± 9.4	159.3 ± 6.1

First of all, none of the samples broke within 5% of strain, that is the upper limit of strain envisaged by ASTM D790-03. This proves the high toughness of the investigated composites. Regarding the comparison between the two samples, the stress-strain curves share the same qualitative behavior, reaching a maximum before a decrease of the sustained stress. Looking at the numerical values in Table 4, it is interesting to observe that the flexural modulus and strength are higher than what reported in the literature for many green composites, and they are in line with the benchmark of glass fiber-reinforced ordinary laminates [22].

The high toughness of the samples was further proved by means of high-velocity flexural tests. Specifically, Charpy-like tests were performed considering an anomalous configuration in which the specimens were struck on the width side to simulate a high speed three-point flexural test. The schematic of the experimental set up is shown in Figure 7a. The results are shown in Figure 7b for representative samples in terms of stress versus strain, where the latter was computed from the deflection data according to the following equation:

$$\varepsilon_f = \frac{6Dd}{L^2} \quad (2)$$

where D is the displacement, L is the span length, and d is the sample thickness.

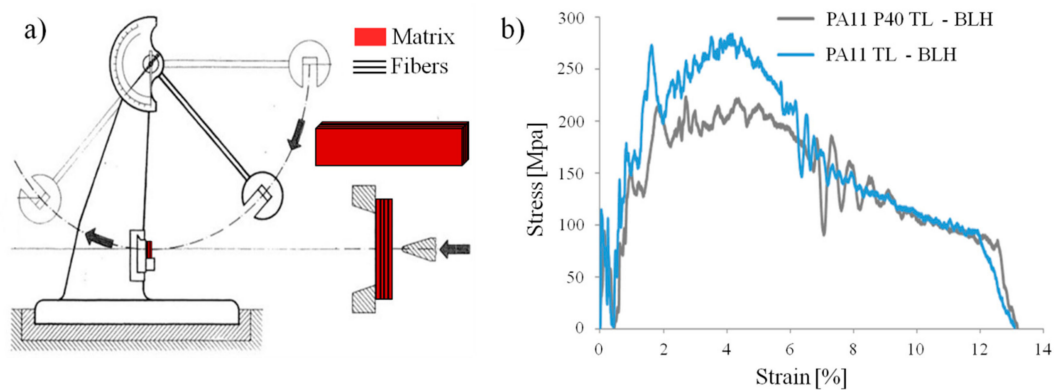


Figure 7. (a) Experimental set-up for the Charpy-like tests. (b) High speed-flexural stress-strain curves of the investigated PA11 composite laminates.

First of all, the results indicate that all specimens did not break during the high-speed flexural test. This further proves the high toughness of the investigated samples, which bend without breaking eventually slipping away. An estimate of the maximum deformation experienced by the samples can be computed through simple geometrical considerations, which lead to a limit deflection of about 39 mm. When properly converted with Equation (2), this value corresponds to about $\varepsilon_f \approx 12\%$ of percentage strain. From a qualitative point of view, the two samples share the same behavior: the stress sharply increases until a maximum at about 4% of strain, and then it gradually decreases. No consideration can be made about the comparison between the rigidity of investigated composite systems, given the usual noise of this kind of curves. However, the performance of the composite based on PA11 P40 TL is only slightly lower than those of the sample based on the PA11 TL in spite of the big differences in terms of the flexural properties of the two matrices.

In order to elucidate the mechanism on the basis of the appreciable flexural properties of the composites based on the plasticized matrix, morphological observations were collected by an optical microscope at the end of the Charpy-like tests. In particular, pictures were taken on the damaged area of impacted specimens, and precisely on the strike face, subjected to compression load, on the corresponding rear side, experiencing tension, and along the thickness direction (Figure 8).

The pictures show that the not plasticized PA11 TL matrix shows clear evidence of damage on the front and rear surfaces of the sample (Figure 8a, picture A and B, respectively), subjected to compression and tension stresses during the impact, respectively. In contrast, the composite based on the tougher PA11 P40 matrix resists without severe damages on the surface polymeric skins (Figure 8b, picture A and B). As a result of the higher flexibility of the plasticized matrix, the breaking mechanisms of fibers are relieved, as well as the crack propagation in the matrix.

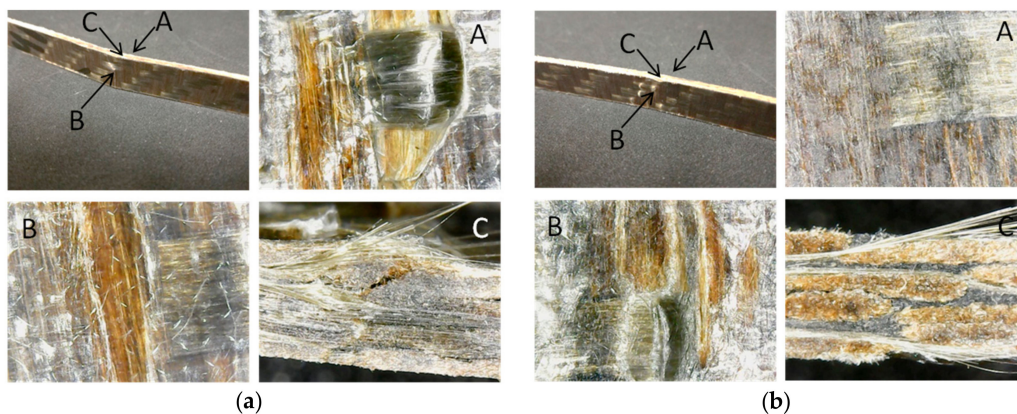


Figure 8. Optical micrographs showing the composite samples based on the not plasticized PA11 TL (a) and plasticized PA11 P40 (b) after the Charpy-like tests. For both figures, the sub figures A, B and C represent the top view, the bottom view and the side view, respectively.

4. Conclusions

Hybrid composite laminates constituted by embedding an interweaved flax and basalt fibers fabric in two polyamide 11 resins, pure and plasticized, were prepared by film stacking and hot-pressing techniques under processing conditions preliminarily optimized by thermal and rheological analyses of the matrices. Specimens of appropriate size, cut from both pure matrix sheets and composite laminates, were subjected to mechanical tests. Specifically, pure resin specimens were studied by quasi-static tensile and flexural tests, while composite specimens were subjected to flexural measurements carried out at both low and high strain rate.

The plasticized matrix exhibited lower stiffness compared to its not plasticized counterpart, but its toughness was more than 50% higher. SEM investigations highlighted a poor polymer-fibers interfacial adhesion in both composites, with detrimental effects in terms of stress transfer ability, but with possible benefits in terms of dissipative phenomena under large deformations. The latter were explored through flexural tests performed at both low and high velocity. When tested under quasi-static conditions, the composites exhibited flexural stiffness and strength higher than those reported in the literature for green composites, and comparable with those of glass-fiber reinforced laminates. Good flexural properties were maintained even under high-velocity conditions, especially for the sample with a plasticized matrix. Overall, the present study demonstrates the suitability of the investigated green composites based on hybrid reinforcement for the manufacturing of items that must meet at least semi-structural requirements, e.g., for panels in the transportation field.

Author Contributions: Conceptualization, P.R. and G.F.; Methodology, P.R.; Formal analysis, P.R. and G.F.; Investigation, L.V. and G.S.; Writing—original draft preparation, P.R. and G.F.; Writing—review and editing, P.R. and G.F.; Supervision, P.R. and G.F.

Funding: This research received no external funding.

Conflicts of Interest: The authors declare no conflict of interest.

References

1. Maries, I.; Kuruvilla, J.; Sabu, T. Mechanical performance of short banana/sisal hybrid fiber reinforced polyester composites. *J. Reinf. Plast. Comp.* **2010**, *29*, 12–29.
2. Manikandan, P.; Chai, G.B. A similitude approach towards the understanding of the low velocity impact characteristics of bi-layered hybrid composite structures. *Comp. Struct.* **2015**, *131*, 183–192. [[CrossRef](#)]
3. Petrucci, R.; Santulli, C.; Puglia, D.; Nisini, E.; Sarasini, F.; Tirillò, J.; Torre, L.; Minak, G.; Kenny, J.M. Impact and post-impact damage characterisation of hybrid composite laminates based on basalt fibres in combination with flax, hemp and glass fibres manufactured by vacuum infusion. *Comp. Part B* **2015**, *69*, 507–515. [[CrossRef](#)]

4. Swolfs, Y.; Gorbatikh, L.; Verpoest, I. Fibre hybridization in polymer composites: A review. *Comp. Part A* **2014**, *67*, 181–200. [[CrossRef](#)]
5. Attia, M.A.; Abd El-Baky, M.A.; Alshorbagy, A.E. Mechanical performance of intra-ply and inter-intraply hybrid composites based on e-glass and polypropylene unidirectional fibres. *J. Comp. Mater.* **2017**, *51*, 381–394. [[CrossRef](#)]
6. Audibert, C.; Andreani, A.S.; Laine, E.; Grandidier, J.-C. Mechanical characterization and damage mechanism of a new flax-kevlar hybrid/epoxy composite. *Comp. Struct.* **2018**, *195*, 126–135. [[CrossRef](#)]
7. Gonzalez, E.V.; Maimi, P.; Sainz de Aja, J.R.; Cruz, P.; Camanho, P.P. Effects of interply hybridization on the damage resistance and tolerance of composite laminates. *Comp. Struct.* **2014**, *108*, 319–331. [[CrossRef](#)]
8. Ying, S.; Mengyun, T.; Zhijun, R.; Baohui, S.; Li, C. An experimental investigation on the low-velocity impact response of carbon-aramid/epoxy hybrid composite laminates. *J. Reinf. Plast. Comp.* **2017**, *36*, 422–434. [[CrossRef](#)]
9. Ferrante, L.; Tirillò, J.; Sarasini, F.; Touchard, F.; Ecault, R.; Vidal Urriza, M.A.; Chocinski-Arnault, L.; Mellier, D. Behaviour of woven hybrid basalt-carbon/epoxy composites subjected to laser shock wave testing: Preliminary results. *Comp. Part B Eng.* **2015**, *78*, 162–173. [[CrossRef](#)]
10. Nisini, E.; Santulli, C.; Liverani, A. Mechanical and impact characterization of hybrid composite laminates with carbon, basalt and flax fibres. *Comp. Part B Eng.* **2017**, *127*, 92–99. [[CrossRef](#)]
11. Lebaupin, Y.; Chauvin, M.; Truong Hoang, T.-Q.; Touchard, F.; Beigbeder, A. Influence of constituents and process parameters on mechanical properties of flax fibre-reinforced polyamide 11 composite. *J. Therm. Comp. Mater.* **2017**, *30*, 1503–1521. [[CrossRef](#)]
12. Oliver-Ortega, H.; Llop, M.F.; Espinach, F.X.; Tarres, Q.; Ardanuy, M.; Mutje, P. Study of the flexural modulus of lignocellulosic fibers reinforced bio-based polyamide 11 green composites. *Comp. Part B* **2018**, *152*, 126–132. [[CrossRef](#)]
13. Oliver-Ortega, H.; Mendez, J.A.; Reixach, R.; Espinach, F.X.; Ardanuy, M.; Mutjé, P. Towards more sustainable material formulations: A comparative assessment of PA11-SGW flexural performance versus oil-based composites. *Polymers* **2018**, *10*, 440. [[CrossRef](#)] [[PubMed](#)]
14. Armioun, S.; Panthapulakkal, S.; Scheel, J.; Tjong, J.; Sain, M. Biopolyamide hybrid composites for high performance applications. *J. Appl. Polym. Comp.* **2016**, *133*, 43595. [[CrossRef](#)]
15. Haddou, G.; Dandurand, J.; Dantras, E.; Mauduc, H.; Thai, H.; Vu Giang, N.; Huu Trung, T.; Pontains, P.; Lacabanne, C. Mechanical properties of continuous bamboo fiber-reinforced biobased polyamide 11 composites. *J. Appl. Polym. Comp.* **2019**, *136*, 47623. [[CrossRef](#)]
16. Fragassa, C.; Pavlovic, A.; Santulli, C. Mechanical and impact characterisation of flax and basalt fibre vinyl ester composites and their hybrids. *Compos. Part B Eng.* **2018**, *137*, 247–259. [[CrossRef](#)]
17. Fiore, V.; Calabrese, L.; Di Bella, G.; Scalici, T.; Galtieri, G.; Valenza, A.; Proverbio, E. Effects of ageing in salt spray conditions of flax and flax/basalt reinforced composites: Wettability and dynamic-mechanical properties. *Comp. Part B Eng.* **2016**, *93*, 35–42. [[CrossRef](#)]
18. Zivkovic, I.; Fragassa, C.; Pavlovic, A.; Brugo, T. Influence of moisture absorption on the impact properties of flax, basalt and hybrid flax/basalt fibre reinforced green composites. *Comp. Part B Eng.* **2017**, *111*, 148–164. [[CrossRef](#)]
19. Zhang, Q.; Mo, Z.; Liu, S.; Zhang, H. Influence of annealing on structure of Nylon 11. *Macromolecules* **2000**, *33*, 5999–6005. [[CrossRef](#)]
20. Agarwal, G.; Reyes, G.; Mallick, P. Study of compressibility and resin flow in the development of thermoplastic matrix composite laminates by film stacking technique. In *ASC Series on Advances in Composite Materials*; Loos, A., Hyer, M.W., Eds.; DESTech Publications: Lancaster, PA, USA, 2013; Volume 6, pp. 215–227.
21. Rilsan Polyamide 11 Brochure. Available online: <https://www.extremematerials-arkema.com/export/sites/technicalpolymers/.content/medias/downloads/brochures/rilsan-brochures/Rilsan-Polyamide-11-Brochure-optimized.pdf> (accessed on 1 March 2019).
22. Pickering, K.L.; Efendy, M.A.; Le, T.M. A review of recent developments in natural fibre composites and their mechanical performance. *Comp. Part A Appl. Sci. Manuf.* **2016**, *83*, 98–112. [[CrossRef](#)]

